Validation of quasi-static Series Hybrid Electric Vehicle Simulation model

Matti Liukkonen*, Ari Hentunen* and Jussi Suomela*
*Aalto University School of Science and Technology, Espoo, Finland
Email: matti.j.liukkonen@tkk.fi

***Abstract*—This paper presents validation measurements of a series hybrid electric vehicle (SHEV) drive line with an ultracapacitor energy buffer. The backward functional quasi-static power transfer plant models in SHEV are discussed and compared against validation measurements. The full power measurement equipment and equipment under tests (EUT) are presented. A traditional road cycle is used to imitate duty vehicles loading in the plant models validation tests. Finally, an energy management algorithm and its behavior are presented, and results are concluded.**

I. INTRODUCTION

THIS study is part of a duty vehicles hybridization project. Hybridization of vehicles and mobile machines aim to decrease emissions and fuel consumption by exploiting kinetic and potential energy of the system, downsizing the primary energy source's power rating, and by generating the primary power with the most efficient means.

Design of a hybrid vehicle or a mobile machine is a very complicated task. Therefore, profound research relating to energy storing, hardware design and supervisory control is needed. This study focuses on hybridization of heavy mobile machines. Thus, the study concentrates on the SHEV drive line topology with a variable speed diesel generator (VSDG), or optionally in the future a fuel-cell (FC) stack, as the primary energy source. [1]

In order to achieve all advantages of the SHEV drive line, proper energy management is needed. Therefore, backward functional quasi-static causal plant models [1] of power transfer components in the SHEV have been developed with Matlab Simulink™ [2]-[3]. Plant models of SHEV components are developed for the rapid control prototyping (RCP) of energy management algorithms [4]. The design of reliably energy management algorithms requires test facilities, where operation of algorithms can be verified before implementation in the target system [5]-[6].

The contribution and novelty of this article is on introducing modeling accuracy of the used simulation method against the behavior of real full-scale hardware, and on essential discussions of full-scale hardware features. Also, conclusions about the behavior of the used hard-computing algorithm for the load-based energy management are made.

The paper is organized as follows. Section II introduces the modeling principles of each power transfer component with the case example comparison between the simulation and the measurement, as well as presents error analysis. Section III presents a discussion of the used energy management algorithm, and section IV concludes the paper.

II. DEVELOPMENT OF SHEV PLANT MODELS

The presented work had its pre-studies published in [2]-[3]. An introduction to the SHEV drive line is presented in Fig. 1, which is an example of an ultracapacitor module (UC) power buffered SHEV drive line. The abbreviations in the figure represent generator (G), active front end converter (AC/DC, AFE), dc-dc converter (DC/DC), inverter (DC/AC) and traction motor (EM). The control signals and actual values are speed reference (ω_{ref}) for the VSDG electronic control unit, power limits of the AFE ($\vec{p}_{\mathrm{limit}}$), the dc link voltage reference for the AFE ($u_{\mathrm{dc\ ref}}$), actual ultracapacitor module voltage (u_{es}), actual dc link voltage (u_{dc}), current reference for the DC/DC (i_{ref}) and actual load power (p_{load}).

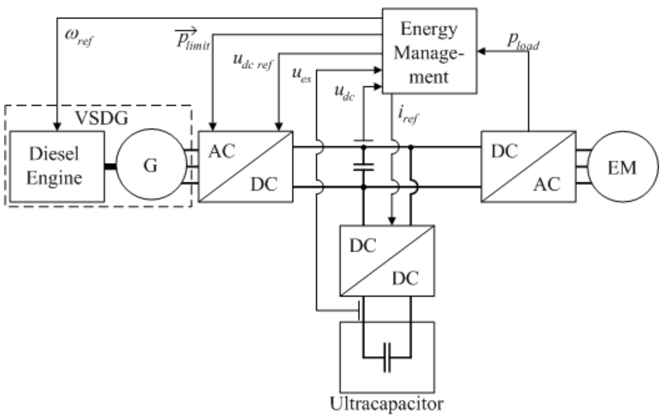

Fig. 1. The SHEV drive line with the ultracapacitor module for power buffering.

978-1-4244-8218-4/10/$26.00 ©2010 IEEE

A. General simulation parameters and starting point

The target of the developed plant models for the SHEV drive line is to envisage 20 Hz-bandwidths events accurately. Furthermore, the designed system level model should be fast to provide efficient energy management RCP [4]. Therefore, backward functional modeling from the imposed load cycle towards the primary energy sources power delivery is appropriate [1].

The starting point of simulation models is to choose a proper simulation time-step, which in the presented cases is 1 ms. The previous fundamental time-step is justified by possible response times of the current control loop in power electronics (PE), for instance, an AFE converter [7]. Furthermore, accurate modeling of a change-over switching in PE components would lead to very low system level simulation times. For this reason, the current control loops of PE components are neglected and it is assumed that PE and EM components transfer the demanded current. Other regulators in different plant-models are operating causality with their input and output delays. Furthermore, the choice of the simulation time-step enforces the plant-models to the functional in the sense of a power electronics description.

In the backward simulations for the SHEV drive line practical starting points are either on the mechanical load of the EMs or the load currents of the inverters. The previous choice is dependent on the available load data. In the case of the mechanical load cycle data, we are able to derivate losses in the EMs and AC/DCs as well as scale loading to electric in the dc link side. This can be achieved with the measurement based efficiency charts in the torque and speed plane, as shown for EM in [5].

In this simulation model validation, the loading is regarded as electrical and derived from the ECE-15 cycle. Figure 2 presents power control targets for both the FC [8] and the VSDG powered SHEVs. The difference between these two cases is on the source current during the cycle's regenerative energy. The shown current waveforms are for the load (i_{load}), the energy storage (ES) (i_{ES}) and the AFE (i_{AFE}).

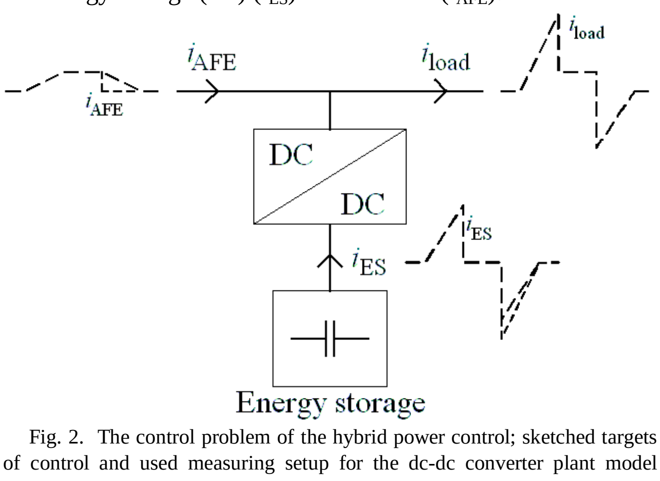

Fig. 2. The control problem of the hybrid power control; sketched targets of control and used measuring setup for the dc-dc converter plant model validation.

B. Measurement equipment and EUTs

Measuring hardware and software of this validation consisted of *dSPACE MicroAutoBox 1401/1505/1507* and *dSPACE ControlDesk* produced by *dSPACE* GmbH, respectively [9]. The measuring time-step for all variables was 10 ms.

The load current measurement was performed with an *LEM/Norma D6100* power analyzer with its triaxial shunts for 6 to 300 A current. The accuracy of the current measurement with the previous shunts is +/-0.1 %. The voltage u_{dc} was measured with the device's terminal with an accuracy of 0.05 %. [10]

The current transducer for the dc-dc converter current measurements was an *LA 305-S* and manufactured by *LEM*. The specific current transducer has a frequency bandwidth (-3dB) of DC to 100 kHz, overall accuracy of +/-0.8 % and less than 0.1 % error due to non-linearity [11].

The voltage transducer in u_{es} measurements was an *AV100-750*, which is also manufactured by *LEM*. The specific voltage transducer has a frequency bandwidth (-3dB) of DC to 13 kHz with less than 0.1 % error due to non-linearity [11].

The EUTs in the validation tests were as follows: The AFE converter *NXA_0460 5*, which is a product of Vacon Plc, regulated the dc link voltage around 650 V and supplied the primary source current i_{AFE}. The dc-dc converter between the dc link and the UC module was produced by MSc Electronics [13], with nominal current of 120A, maximum current of 200A and minimum current of 20A in the ES voltage level. The UC module was a product of *Maxwell technologies*®, with a nominal capacitance of 17.8 F and maximum voltage of 390 V [14].

C. Loading of the test system

In the simulation validation tests the load of the dc link was created with inverter, which was controlling one side of an EM dynamometer. The load current (i_{load}) was realized with speed control mode of a loading EM and torque control mode with the cascaded power controller of a traction motor. The traction motor power reference was ECE-15 drive cycle based. The structure of the used dynamometer is described in [5].

Figure 3 presents the speed pattern of the ECE-15 drive cycle, measured load current of the EM dynamometer and the AFE current in the dc link voltage level, as well as the ES current in the energy storage's voltage level.

The measured load current was used also as a loading of the dc link in the simulation model validation. This was done because modeling of the load would be very complicated and is not necessary for the power management design in non-predictive load-power-based-causal control. The ES current is the result of the supervisory control algorithms for the dc-dc converter in current control mode, and the AFE current is a derivative of the load current and the ES current.

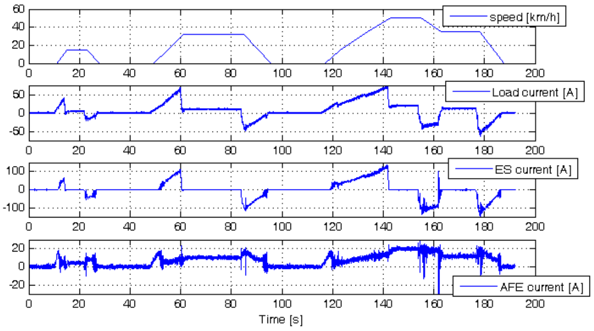

Fig. 3. Speed pattern of the ECE-15 drive cycle, the measured load current, the ES current and the resulting AFE current.

D. Functional plant model of the dc-dc converter

The PE converters typically reach to very high efficiency values in their best operation area. On the contrary, the efficiency of the PE converter can degrade significantly, if an inappropriate operation area is used. Therefore, with the previous presumption from the simulation time-step it is necessary to simulate the dc-dc converters with a combination of a measurement based efficiency map and a functional description.

The efficiency of dc-dc converter in general depends on the transferred current and the voltage conversion ratio. Hence, in the study [3] have been investigated efficiencies, which can be reached in power transfer with the previous variables.

The essential functionalities and dynamical properties which can be programmed on the dc-dc converter plant model are current control response time, minimum current, current ripple or noise, conduction event of the change-over switches' anti-parallel diode, quadruple point voltage controller and power losses according to the operation point.

Figure 4 shows how the plant model follows the original EUTs´ current with the same loading (i_{load}) in the simulation model as in the measurement. The measurement setup is as shown in Figure 2. The dc-dc converter current is presented in the ES voltage level and it corresponds to the ES current.

It can be seen from Figures 4 and 5 that there is some difference and variance between the simulated plant models´ current and the EUTs´ current, but it is convenient that the energy content of the difference is vanishing. The maximum current difference is 150 A, the mean error is -0.32 A and the rms error is 5.7 A. Furthermore, the mean error scale is near to the linear error and the rms error is near to the overall error of the sensor in the measuring range.

The largest differences between the measured and the simulated currents can be noticed near the minimum current (20 A) of the dc-dc converter (1), the highest regenerative current values (2) and during the shut off of the regenerative current (3). The previous numbers refer to areas in the scale-up Figure 5.

Points 2 and 3, in Figure 5, come up because of the energy management algorithm and the AFE voltage regulator is acting to stabilize the dc link voltage. The exact behavior of the AFEs´ voltage regulator is difficult to reproduce with the used functional simulation method. Therefore, the dc link voltage variation interacts with the measurement result. The dc link voltage drop at point 3 can be seen in Figure 6. The dc link voltage drop in this case was enforced with the low generating power limit of the AFE. The dc link voltage drop against the generating power limit could not be reproduced with the used simulation approach.

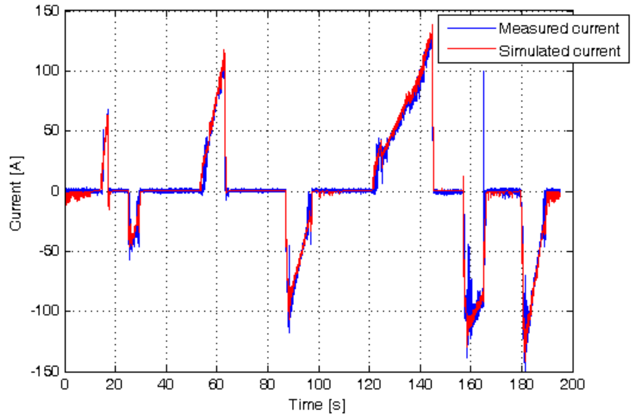

Fig. 4. The overview of the measured and the simulated dc-dc converter currents.

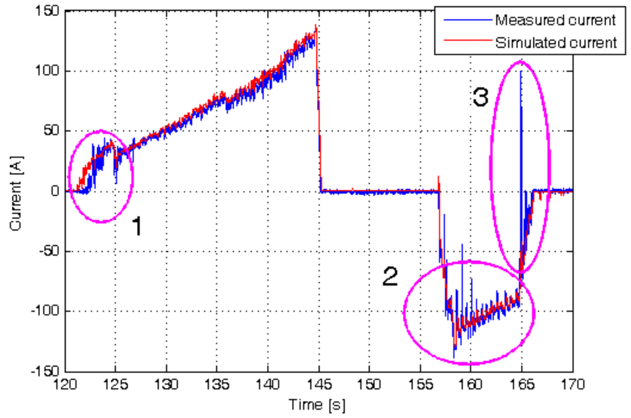

Fig. 5. The scale-up of the measured and the simulated dc-dc converter current.

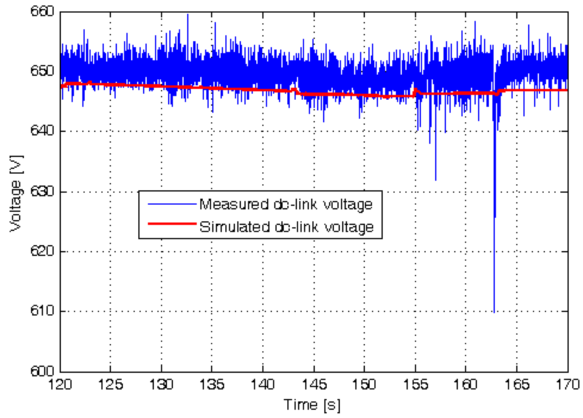

Fig. 6. The measured dc link voltage during the simulation model validation.

E. Functional plant model of the AFE

The active-front-end converter in the system level model is modeled with the efficiency map in the torque and speed plane, and also with the voltage regulator, which controls dc-current to the dc link. Losses of the generator are taken into account respectively. Change of voltage regulator type and parameters affect how power transfer is realized. In the developed AFE functional plant model the considered aspects of the voltage regulator are the stiffness of the voltage in the dc link side, as well as the control response time.

In the presented simulation model validation measurements the AFE took power directly from the power distribution network. Even though the power limit of the AFE was set to low (15.7 kW ~24 A) to prevent too strong supply, still the dc link voltage variation was low. Under stable conditions the dc link voltage was around 650 V +/-10 and in some transients, which are pointed out in Figure 6, the dc link voltage dropped down to 610 V. This affected the dc-dc converter current shown in Figures 4 and 5.

The next figures present the indirectly measured current of the AFE compared against the corresponding simulated current. The AFE current was achieved by calculating the difference between the load current and the dc-dc converter current due to practical reasons. First, Figure 7 presents the overview of the AFE current, and Figure 8 presents the scale-up of the current transients.

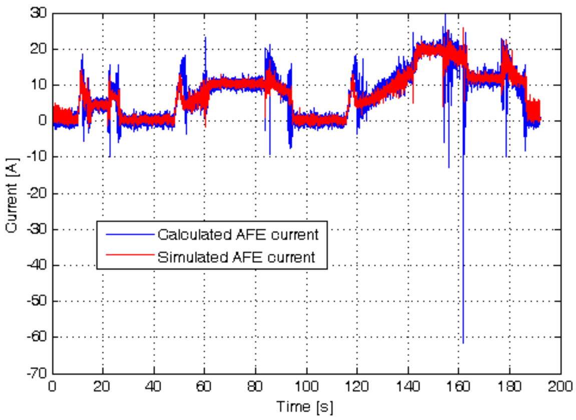

Fig. 7. The calculated and the simulated current of the AFE.

The scale-up figure shows the affect of the dc-dc converter minimum current (1), the accuracy of the load current sharing algorithm (2) and how current flows to the dc link from the AFE, if the generating power limit is not changed (3 and 4). The previous areas are shown in the scale-up figure. The maximum current difference, between the measured and simulated AFE current, is 79.8 A, the mean error is -0.19 A and the rms error is 3.0 A. The mean error is comparable to linear measurement accuracy and rms error to overall accuracy as earlier in the current measurement.

The size of load-step for the AFE in area 2, shown in Figure 8, depends on the pattern of the loading and energy management algorithm's parameters. So, the loading conditions should be taken under consideration in the energy management algorithm in order to optimize load sharing during the acceleration event.

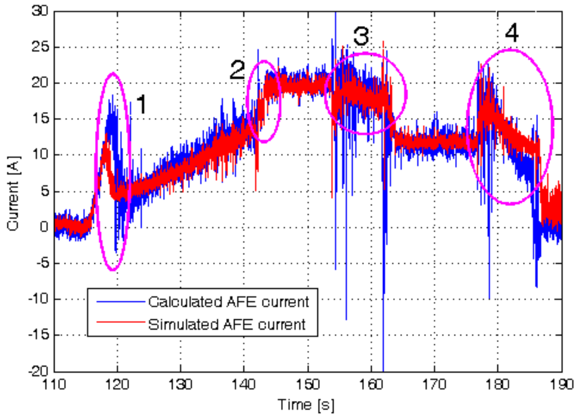

Fig. 8. The scale-up of the measured and the simulated current of the AFE.

F. Modeling of the ultracapacitor module

An UC simulation model is based on equivalent series resistance (R_{dc}) and measured capacitance variation as a function of ES voltage and current. The function for simulating the ES voltage is shown in Equation 1, where C_{es} represents the capacitance of the ES, i_{es} represents ES actual current and Δt represents the discrete time-step of simulations

$$u_{es}(R_{dc}, C_{es}(u_{es}, i_{es})) = R_{dc} i_{es} + \Delta t * i_{es} / C_{es}(u_{es}, i_{es}). \tag{1}$$

The figure below presents two different cases from the simulated and the measured voltage variation of the UC module with charging, discharging and static events. One simulation case is for constant nominal capacitance of the UC module, and other is for variable capacitance model simulation. The simulated cases of UC voltages are the integrals of the simulated dc-dc converter current.

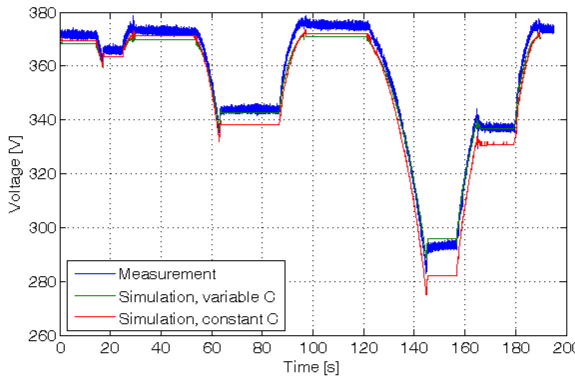

Fig. 9. Two different simulation cases from the UC modules´ voltages ($C_{constant}$ and $C_{variable}$) and the measured voltage with the same ES current.

Reasonable simulation accuracy is achieved even with the nominal capacitance of the UC module (error values: max 14 V, mean 4.8 V and rms 5.6 V), but smaller error values are achieved with the measured capacitance variation based model (max 8.4 V, mean 1.7 V and rms 3.0 V). Still, the mean error is approximately a decade larger than linear measurement error in measuring range.

G. Modeling of the diesel engine

The simulation model validation with measurements has been divided into testing of the electrical energy management and testing of the VSDG responses. This section presents a comparison of the simulation and logged parameter values from the VSDG electronic control unit. Realized loading of the VSDG has been used as a load torque in the simulation model. Both, the load-step and speed-reference-step responses are considered.

The diesel engine simulation model includes Newton's second law for rotational dynamics, the PI-controller for speed, the rate limiter for the speed reference, idle losses as a function of speed and calculation of fuel consumption from the PI-controller's fuel injection output and actual speed. The diesel engine under comparison is a 49 DTAG, and it is manufactured by AGCO SISU POWER [15].

Figure 10 presents the actual load torque during the load-step response test, a comparison between the simulated and the logged speed, as well as the speed reference. An accurate simulation of the speed response in load-steps depends on the PI-controller parameters. With the used PI-controller parameters the speed error values were as follows: max 91 rpm, mean 4.9 rpm and rms 8.8 rpm. These values are determined from an evaluation run of 300 seconds. The high maximum error is caused by misalignment between simulated and measured transients. Otherwise, the measurement accuracy is dependent on the features of the target equipment.

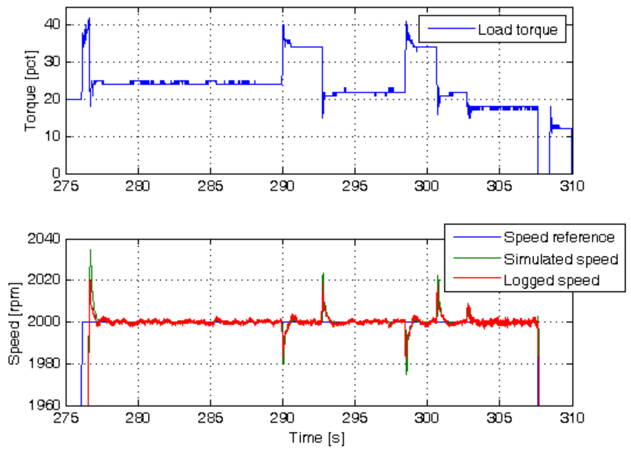

Fig. 10. The comparison between the simulation model and the measurement in the load-step response test.

Figure 11 presents the speed-reference-step responses for acceleration as well as for deceleration.

In the acceleration event the step-response depends on the speed reference rate limiter and the over-shoot depends on the PI-controller parameters. In the deceleration event the step-response depends on the inertia of the shaft, idle losses and the loading. In the previous case the loading can be seen from Figure 10 and in the latter case the loading was zero.

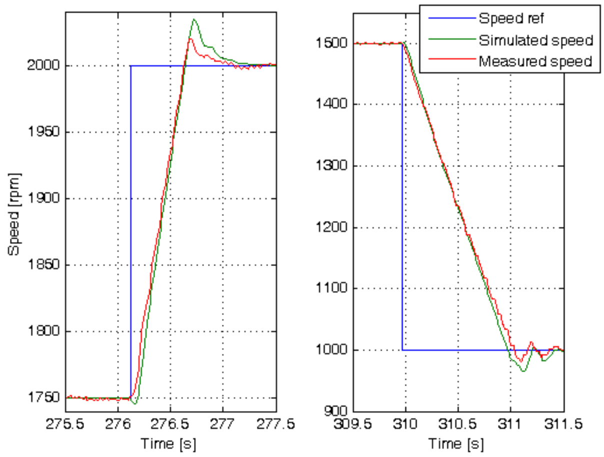

Fig. 11. The comparison between the simulation model and the measurement in the speed-reference-step test.

III. Energy Management Algorithm

This section presents a hard-computing algorithm, which was used for energy management of the SHEV system model in the validation tests with one ES. The presented energy management is targeting to peak power shaving from the primary energy source.

The energy management algorithm's (Fig. 12) inputs are, as defined with context of Fig. 1, $u_{\mathrm{dc\ ref}}$, u_{dc}, p_{load} and u_{es}. The output of the algorithm is i_{ref}. The moving average of the algorithm had unity coefficients and was calculating a 20 seconds average from the load power. The weight vector w_1 changes actual power to a per-unit value and w_2 defines the power which should be generated with the VSDG as a function of the actual ES voltage. The positive-linear function prevents filtered power calculation from going negative, and, therefore, all regenerative power is included in the load sharing algorithms output. The P-controller from the dc link voltage stabilizes the dc link and can be used for charging the ES.

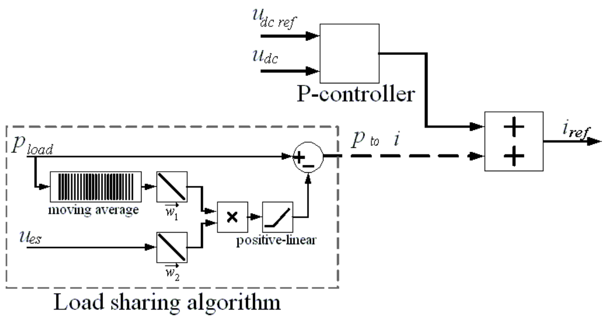

Fig. 12. Hard-computing algorithms for energy management in the SHEV drive line

We can discover that the proposed hard-computing algorithm is capable to realize all operation modes presented in [16] for the series hybrid drive train. Therefore, the study suggests that the power management of the SHEV drive line can be designed using the discussed hard-computing algorithms with use of finite-state machines or soft-computing algorithms.

Figure 13 specifies operation modes, which are realized with the proposed algorithm. Pure electric and engine modes come naturally, as well as pure ES charging mode. Hybrid mode (1) operates while the presented algorithm is running. Engine traction and ES charging mode (2) can be achieved, for example, with the change of voltage reference or the algorithm's weight vector w_2. Regenerative braking mode (3) operates with the algorithms nature, when the power limits of the AFE are controlled to zero. Hybrid ES charging mode (4) realizes when the algorithm is running and the power limits of the AFE are controlled appropriately.

In Figure 13, the dc link voltage drop in the operation area 2 is due to a voltage reference change for the proposed algorithms P-controller in order to charge the ES. Correspondingly in operation area 3, the drop is caused by the parallel current controllers of the algorithm regulating the current reference simultaneously.

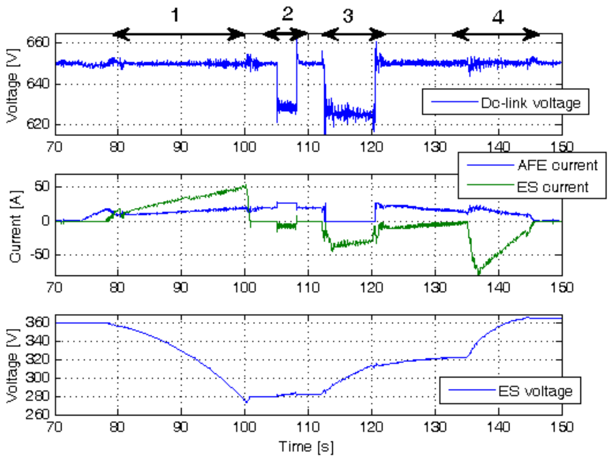

Fig. 13. The simulation figure presents different operation mode areas in the hybrid drive.

IV. CONCLUSION

This study discussed realization of backward functional quasi-static causal plant models of the SHEV, the verified simulation methods' accuracy with the introduced full-scale hardware and the proposed load-based energy management algorithms for the SHEV. In addition, relevant full-scale hardware features for RCP plant-models were discussed.

The used simulation method derivates accurately the mean values, as well as rms values, of all modeled variables. On the other hand, some transients of variables could not be reproduced as in cases which were caused by unknown regulator parameters, simplifications of models or misaligned control moments respect to validation. Therefore, maximum errors during transients remain high. However, the simulation accuracy is on a good level for a complex system. This can be justified with the insignificant energy content of the mean error values. Besides, the represented measuring errors are not significant compared to the simulation errors.

The proposed load-based hard-computing algorithm shows promising results for use in the SHEV energy management. However, realization of hybrid mode in peak power shaving during acceleration and deceleration is dependent upon the load pattern. Therefore, further study could be made to improve the algorithm to adapt in to different load pattern conditions. In addition, all required operation modes for the SHEV drive line energy management were described in the simulation with the proposed algorithm.

This study's aim is on duty vehicles hybridization, which have diverse and in some cases very repetitive load cycles. The previous brings opportunities for the energy management design.

ACKNOWLEDGMENT

This study has been carried out in HybDrive, TopDrive and HybLab projects financed by the Finnish Funding Agency for Technology and Innovations (Tekes) and Multidisciplinary Institute of Digitalization and Energy (MIDE) of Aalto University School of Science and Technology, respectively.

REFERENCES

[1] C. C. Chan, A. Bouscayrol and K. Chen, "Electric, Hybrid, and Fuel-Cell Vehicles: Architectures and Modeling," IEEE Trans. Veh. Technol., vol. 59, no. 2, pp. 589-598, Feb. 2010.

[2] M. Liukkonen, A. Hentunen, J. Suomela and J. Kyyrä, "Functional Simulations of Power Electronics Components in Series-Hybrid Machinery for the needs of OEM," presented at the NORPIE, Nordic Workshop on Power and Ind. Electronic**s**, Espoo, Finland, Jun. 9-11, 2008.

[3] M. Liukkonen, A. Hentunen, J. Suomela and J. Kyyrä, "Low-pass Filtered Power-flow Control in Series Hybrid Electric Vehicle," presented at the EVS24 Int. Battery, Hybrid and Fuel Cell Electric Vehicle Symp., Stavanger, Norway, May 13-16, 2009.

[4] M. Broy, I. H. Kruger, A. Pretschner and C. Salzmann, "Engineering Automotive Software" Proc. of the IEEE, vol. 95, no. 2, pp. 356-373, Feb. 2007.

[5] A. Hentunen, J. Suomela, A. Leivo, M. Liukkonen and P. Sainio, "Hardware-in-the-Loop Verification Environment for Heavy-Duty Hybrid Electric Vehicles," IEEE Vehicle Power and Propulsion Conf., Lille, France, Sep. 1-3, 2010, unpublished.

[6] Y. Cheng, J. V. Mierlo and P. Lataire, "Research and test platform for hybrid electric vehicle with the super capacitor based energy storage," European conf. on Power Electron. and Applications, Aalborg, Denmark, Sep. 2007.

[7] M. Gokasan, S. Bogosyan and D.J. Goering, "Sliding Mode Based Powertrain Control for Efficiency Improvement in Series Hybrid-Electric Vehicles," IEEE Trans. on Power Electron. vol. 21, pp. 779-790, May 2006.

[8] J. V. Mierlo, Y. Cheng, J.-M. Timmermans and P. V. Bossche, "Comparison of Fuel Cell Hybrid Propulsion Topologies with Super-Capacitor," Power Electron. and Motion Control Conf. EPE-PEMC, Portorož, Slovenia, Aug. 2006.

[9] dSPACE homepage. [Online]. Available: http://www.dspace.de/

[10] Norma D6000 specification description. [Paper].

[11] LEM homepage. [Online]. Available: http://www.lem.com/

[12] Vacon homepage. [Online]. Available: http://www.vacon.com/

[13] MSc Electronics homepage. [Online]. Available: http://www.mscelectronics.fi/

[14] Maxwell Technologies homepage. [Online]. Available: http://www.maxwell.com/

[15] AGCO Sisu Power homepage. [Online]. Available: http://www.agcosisupower.com/

[16] M. Ehsani and Y. Gao, "Hybrid Drivetrains," in Handbook of Automotive Power Electronics and Motor Drives, Boca Raton, FL: T&F, 2005, ch. 1, sec. 3, pp. 37-53.